RNA BIOLOGY
2021, VOL. 18, NO. S1, 382–396
https://doi.org/10.1080/15476286.2021.1950980

Taylor & Francis
Taylor & Francis Group

RESEARCH PAPER

Structural and functional insights into human tRNA guanine transglycosylase

Katharina Sievers[a], Luisa Welp[b], Henning Urlaub[b,c], and Ralf Ficner [a,d]

[a]Department of Molecular Structural Biology, University of Göttingen, Göttingen, Germany; [b]Bioanalytical Mass Spectrometry Group, Max Planck Institute for Biophysical Chemistry, Göttingen, Germany; [c]Bioanalytics Group, Institute for Clinical Chemistry, University Medical Center Göttingen, Göttingen, Germany; [d]Cluster of Excellence "Multiscale Bioimaging: From Molecular Machines to Networks of Excitable Cells" (Mbexc), University of Göttingen, Göttingen, Germany

ABSTRACT

The eukaryotic tRNA guanine transglycosylase (TGT) is an RNA modifying enzyme incorporating queuine, a hypermodified guanine derivative, into the tRNAs^{Asp,Asn,His,Tyr}. While both subunits of the functional heterodimer have been crystallized individually, much of our understanding of its dimer interface or recognition of a target RNA has been inferred from its more thoroughly studied bacterial homolog. However, since bacterial TGT, by incorporating queuine precursor preQ$_1$, deviates not only in function, but as a homodimer, also in its subunit architecture, any inferences regarding the subunit association of the eukaryotic heterodimer or the significance of its unique catalytically inactive subunit are based on unstable footing. Here, we report the crystal structure of human TGT in its heterodimeric form and in complex with a 25-mer stem loop RNA, enabling detailed analysis of its dimer interface and interaction with a minimal substrate RNA. Based on a model of bound tRNA, we addressed a potential functional role of the catalytically inactive subunit QTRT2 by UV-crosslinking and mutagenesis experiments, identifying the two-stranded βEβF-sheet of the QTRT2 subunit as an additional RNA-binding motif.

ARTICLE HISTORY
Received 23 April 2021
Revised 21 June 2021
Accepted 29 June 2021

KEYWORDS
Queuine; tRNA modification; RNA-binding protein; transglycosylase; heterodimer; eukaryotic; structural biology; X-ray crystallography

Introduction

Queuosine (Q) is an extensively modified nucleoside found at position 34, the wobble position, of tRNA^{Asp}, tRNAs^{Asn}, tRNA^{His} and tRNA^{Tyr}, the isoacceptors decoding NAC and NAU codons [1]. In these positions, it is almost universal among both bacteria and eukaryotes.

Queuosine-modification has been shown to regulate translational speed by inverting a tRNA's preference for C- or U-ending synonymous codons, although the direction of this preference seems to depend both on species and codon type [1–5]. In *Shigella flexneri*, a bacterium causing shigellosis, queuosine deficiency leads to a loss of virulence, possibly because its *virF* mRNA is itself Q-modified [6,7]. Among eukaryotes, the presence of queuosine at tRNA position 34 is stimulatory of the methyl transferase Dnmt2 [8,9] and inhibits the 'tRNase' angiogenin [10].

Chemically, queuosine is a guanosine derivative comprised of a 7-deazapurine core and a cyclopentenediol moiety attached via a 7-aminomethyl linker [11,12]. The biosynthesis of queuosine requires eight enzymes in bacteria: Five of them are responsible for converting guanosine 5′-triphosphate (GTP) into the precursor 7-(aminomethyl)-7-deazaguanine (preQ$_1$) [13–19], the enzyme tRNA guanine transglycosylase (TGT) then inserts preQ$_1$ into position 34 of a substrate tRNA, where it replaces the genetically encoded guanine [20,21]. The final two reactions converting preQ$_1$ into queuosine then occur in the context of the tRNA [22–29].

The bacterial TGT enzyme is a homodimer, each subunit is a modified $(\beta/\alpha)_8$ barrel with multiple insertions, including a zinc-binding domain, which coordinates a single Zn^{2+} ion [30,31]. At the centre of the symmetric dimer interface, two loop-helix motifs form a network of polar interactions with two extensive helix-turn-helix motifs framing the zinc-binding domain of the opposing subunit [32,33]. However, the primary contribution to dimer stability are two aromatic hot spots located in the peripheries of the interface [33,34]. Due to the geometry of the dimer, only one subunit is catalytically active at a time because a tRNA molecule being bound and converted by one subunit blocks the active site of the other by steric hindrance [35,36]. The TGT reaction follows ping-pong kinetics: First, a covalent intermediate is formed between a catalytic aspartate and ribose 34 of the tRNA substrate, leading to the release of free guanine, before preQ$_1$ can take its place in the active site and be incorporated into the tRNA, thus completing the reaction [37].

Although queuosine is found in the tRNAs of most eukaryotes, TGT is the only enzyme of the Q-biosynthesis pathway with a eukaryotic homolog. Instead of producing queuosine and its precursors *de novo*, eukaryotes salvage its free base queuine from gut bacteria or nutritional sources [38–43]. For this reason, the eukaryotic TGT is adapted to insert the fully modified queuine instead of its precursor preQ$_1$ into the tRNA substrate [44–46]. In mammals, queuosine can be further modified by mannosylation or galactosylation [47,48]. Unlike bacterial TGT, eukaryotic TGT is a heterodimer and is comprised of a catalytically active subunit (QTRT1) and a catalytically inactive one (QTRT2) [49,50]. With the exception of a modified binding pocket to

CONTACT Ralf Ficner rficner@uni-goettingen.de Department of Molecular Structural Biology, University of Göttingen, Göttingen, Germany
Supplemental data for this article can be accessed here

accommodate the bulky cyclopentenediol moiety of queuine, the structure of QTRT1 is very similar to bacterial TGT [51]. The catalytically inactive QTRT2 is homologous and shares the overall $(\beta/\alpha)_8$ fold architecture, but its active site and several other structural elements are degenerate or modified [52].

Since both subunits of the eukaryotic TGT are homologs of the bacterial TGT, it is likely that their dimerization follows its model. However, the lack of a crystal structure has so far impeded thorough understanding of the heterodimer's subunit arrangement.

Detailed knowledge of the dimer is also necessary to understand how TGT enzymes bind their substrate tRNAs. Footprinting data of bacterial TGT suggests interaction mainly with the tRNA's anticodon arm [53]. Experiments with *in vitro* transcribed minimal RNA constructs confirmed that a stable stem loop with a $Y_{32}U_{33}G_{34}U_{35}$ sequence in a 7-membered loop is sufficient to be recognized and converted by bacterial TGT [54,55]. Such a stem loop RNA was used in the only crystal structure of RNA-bound TGT, which revealed a drastically changed conformation of the anticodon loop and specific recognition of the $U_{33}G_{34}U_{35}$ bases, while the remainder of the RNA was bound independent from sequence via its sugar-phosphate backbone [35]. The only data addressing the substrate specificity of eukaryotic TGT is based on *in vivo* experiments using a *Xenopus* oocyte model which suggest that queuine is only incorporated into tRNAs with intact three-dimensional architecture [56,57]. This is in contrast to the minimalist substrate requirements of bacterial TGT and raises the question of whether the eukaryotic TGT·RNA complex differs from the bacterial one.

Here, we present the first crystal structure of human TGT in its heterodimeric and RNA-bound form, serving not only to understand subunit association in eukaryotic TGT but also its interaction with and recognition of a stem loop RNA substrate. In addition, we performed UV-crosslinking and mutagenesis experiments on which we based a model of how a full tRNA is bound by human TGT.

Results

Crystal structure of a human TGT·RNA complex

In preparation for crystallization of a human TGT·RNA complex, we assembled a complex of heterodimeric TGT and a 25-mer stem loop RNA containing a '$Y_{32}U_{33}G_{34}U_{35}$' anticodon loop sequence [35]. Such a stem loop RNA is the known minimal substrate for bacterial TGTs [55] but we verified that *in vitro* it is also converted by the human TGT (S 1). For crystallization, the complex was assembled in the presence of excess 9-deazaguanine (9dzG) to chemically trap the covalent TGT-RNA intermediate [35].

We obtained rod-shaped crystals from PEG (1500, 3350 or 4000)-based crystallization conditions at pH 5.5–6.5. Crystals appeared after 2–4 days, reached up to 150 µm in size and grew at both 4°C and 20°C. We collected datasets of diffraction images from several crystals using synchrotron radiation and identified the crystals to belong to either space group C2 or $P2_1$.

We obtained initial phases by molecular replacement using the structures of human QTRT1 (PDB-ID: 6H42) and mouse QTRT2 (6FV5) as search models. Although various search combinations were tried, only the heterodimeric form led to drastically improved R-factors during initial refinement. Manual inspection of the resulting electron density revealed a large volume of additional density in which the stem loop RNA was placed (S 2). The best dataset (from crystal grown in 0.1 M MMT pH 6, 25% (w/v) PEG 1500 at 4°C) was refined at a resolution of 2.88 Å and to R-factors of 21.17% (R_{work}) and 24.84% (R_{free}) (Table 1).

The asymmetric unit contains one RNA molecule and two polypeptide chains (QTRT1 and QTRT2), each coordinating a Zn^{2+} ion (Fig. 1A). 9-Deazaguanine (9dzG) is bound to the active site of QTRT1. The first 15 amino acid residues of chain A (QTRT1) are missing, although two of them are remnants of the cleaved N-terminal His-tag and numbering of the model therefore starts with P14. The model is complete at both the QTRT1 C-terminus and the QTRT2 N-terminus, and only the very last residue (S415) is missing from the QTRT2 C-terminus. Other areas of missing density will be discussed below.

Both subunits in this new structure of RNA-bound human TGT (hTGT) have the fold that is characteristic for TGT proteins and which consists of a central $(\beta/\alpha)_8$ barrel with several insertions, including a zinc-binding domain. For this reason, we have adapted the established nomenclature [35,52] to refer to their secondary structure elements (See S 3 for a topology diagram). There is continuous density linking ribose 34 and the catalytic aspartate 279 while the density for 9dzG has no connection to the RNA (Fig. 1B). It is therefore clear that the structure does indeed represent the covalent TGT-RNA intermediate.

Table 1. Data collection and refinement statistics

Data collection	
X-ray source	Synchrotron (BESSY II, MX 14.1)
Wavelength (Å)	0.9184
Resolution (Å)	50.00-2.88
Space group	C121
a, b, c (Å)	161.84, 56.96, 102.96
α, β, γ (°)	90.0, 124.93, 90.0
Wilson B ($Å^2$)	67.81
R_{meas} (%)[1]	11.6 (112.1)
I/σ (I)[1]	13.83 (1.81)
$CC_{1/2}$[1]	99.9 (87.6)
Completeness (%)[1]	98.9 (99.8)
Redundancy	6.7
Refinement	
Resolution (Å)	42.20-2.88
No. of reflections	16550
R_{work} (%)	21.17
R_{free} (%)	24.84
Mean B value ($Å^2$)	88.54
Protein	88.78
RNA	86.24
R.m.s. deviations	
Bonds (Å)	0.008
Angles (°)	1.414
Ramachandran favored (%)	96.21
Ramachandran outliers (%)	0.00
Rotamer outliers (%)	4.6
Clash score	7.91

[1]Numbers in parentheses are for the highest resolution shell.

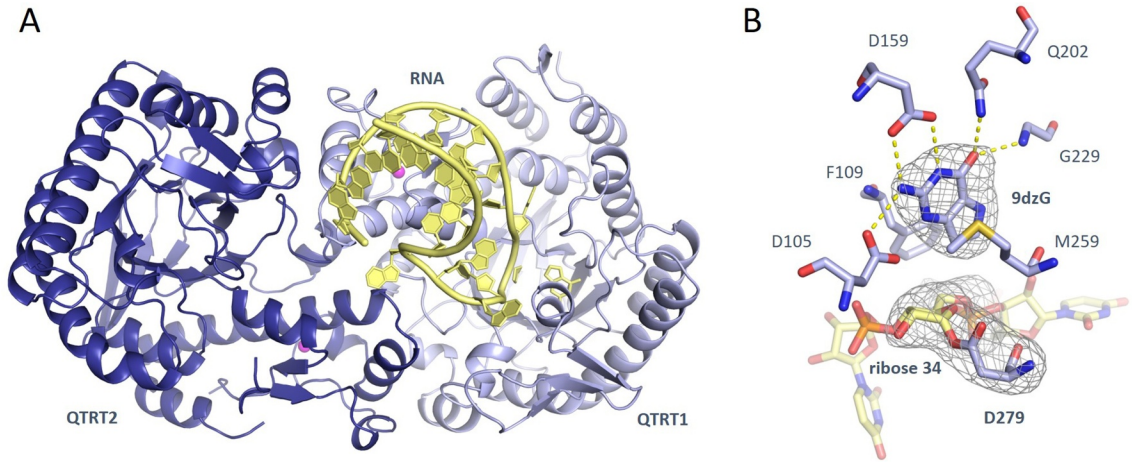

Figure 1. Crystal structure of human TGT with covalently bound RNA.

A: Structural overview of the heterodimeric TGT from *Homo sapiens* as a covalent intermediate with a 25-mer RNA stem loop. The catalytic subunit (QTRT1) is shown in light blue, the non-catalytic subunit (QTRT2) is shown in dark blue, the RNA stem loop is shown in yellow. The 9dzG molecule bound at the active site is shown in yellow stick representation. The two Zn^{2+} ions are depicted as pink spheres. **B**: Active site of human TGT with ribose 34 covalently bound to catalytic aspartate 279 and 9dzG coordinated by D105, F109, D159, Q202, G229 and M259. An mFo-DFc electron density omit map for D279, ribose 34 and 9dzG contoured at σ = 5.0 is shown as a grey mesh.

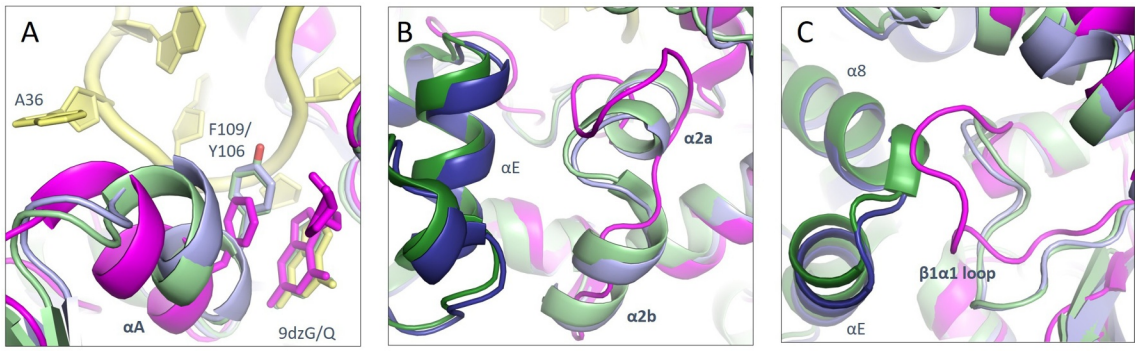

Figure 2. Conformational rearrangements of hTGT.

Comparison of hTGT structure (blue and yellow) with queuine-bound QTRT1 (PDB-ID: 6H45, depicted in pink) and RNA-bound bacterial TGT (PDB-ID: 1Q2R, depicted in green). **A**: Conformational shift of QTRT1 helix αA and equivalent residues F109/Y106 (human/*Zymomonas mobilis*) upon RNA binding. **B**: Formation of QTRT1 helices α2a and α2b upon dimerization. **C**: Re-orientation of QTRT1 β1α1 loop at dimer interface and interaction with helices αE and α8 of the opposing subunit (QTRT2/bacTGT).

The 9dzG base co-locates with that in the bacterial structure of a covalent RNA intermediate (PDB-ID: 1Q2R) and the 7-deazaguanine moiety in the structure of human QTRT1 soaked with queuine (6H45) [35,51]. The surrounding active site is largely identical to the available QTRT1 structures 6H42 and 6H45 which represent its apo and queuine-bound form. One of the few differences between these two structures is the conformation of S231 and G232 which are flipped to accommodate queuine's cyclopentenediol moiety in 6H45. In the RNA-bound hTGT structure, the G/Q binding pocket is occupied by 9dzG, which lacks the cyclopentenediol extension, and, while showing some flexibility, S231 and G232 occupy positions most similar to the apo structure.

Other parts of the QTRT1 subunit have more severely altered conformations compared to the apo structure: Helix αA (108–113), which is located near the active site, is shifted closer to the 9dzG base bound at the catalytic centre (Fig. 2A). This new position is identical to that occupied by the equivalent helix in the structure of RNA-bound TGT from *Zymomonas mobilis* (1Q2R), while in RNA-free structures of the bacterial homodimer (e.g. 1PUD), helix αA co-locates with those of the human QTRT1 subunit (6H42, 6H45) [30,35,51], illustrating that this change is caused by binding of the RNA rather than dimerization. The position of adenine 36 right at the end of helix αA deems it responsible for its displacement. Within the helix, residues Q110 and S113 form hydrogen bonds with the phosphate backbone of nucleotides 35 to 36. Helix αA also contains F109 which is partly responsible for stabilizing the base in the active site via pi-stacking interaction.

Amino acid residues 74–89, unstructured in the non-dimeric QTRT1 structures, form two helices α2a and α2b in the structure of hTGT (Fig. 2B). Despite being in close vicinity to U35, this change seems to be a result of heterodimerization as equivalent helices are present not only in the bacterial RNA-bound structures but also in structures of the RNA-free bacterial homodimer [30,35].

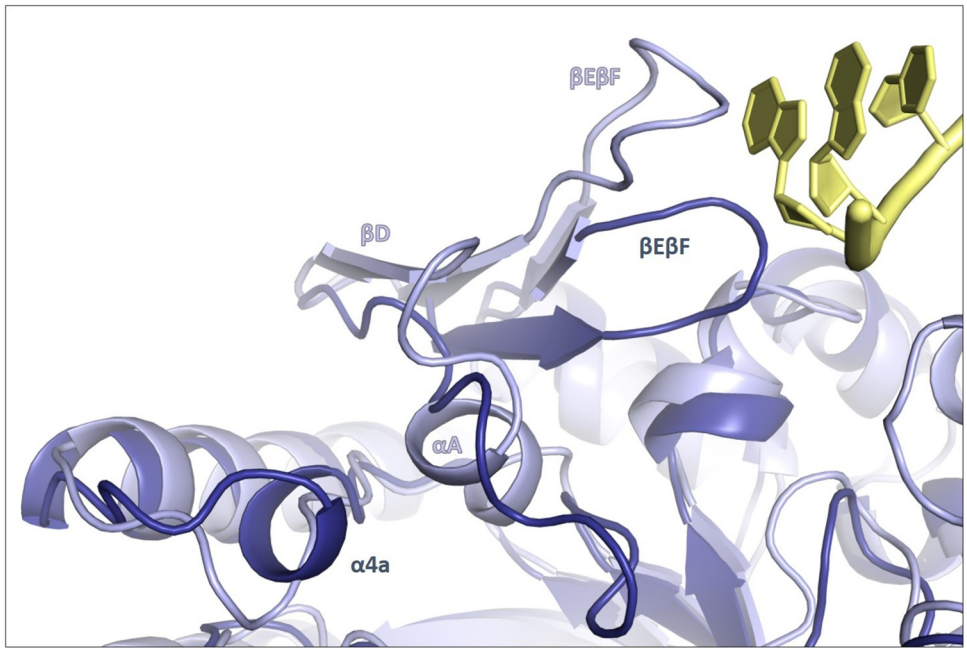

Figure 3. Structural differences between QTRT1 and QTRT2.
The comparison of QTRT2 (dark blue) with superimposed QTRT1 (light blue) reveals altered secondary structure elements in the region near the 5′ end of the stem loop RNA (yellow). QTRT2 secondary structure elements are labelled in dark blue, QTRT1 elements are labelled in light blue.

Similarly, the QTRT1 loop-helix motif composed of β1α1-loop [47–58] and preceding helix α1 [59–65] take a different course in the hTGT structure (Fig. 2C) while the sharply angled turn between helices αE and α8 (327–335 and 339–366) of the same subunit is slightly twisted. Both of these motifs are part of the dimer interface and occupy identical positions in structures of the bacterial dimer [30]. The altered position of helix αE also causes a small change in the neighbouring loop containing residues 301–311 which is also identical to that in bacterial dimers [30,35]. This loop contains several positively charged amino acid residues and acts as a platform for the backbone of nucleotides 29–32.

The new hTGT structure is the first crystallographic representation of the human non-catalytic subunit QTRT2. However, upon inspection it immediately becomes clear that it is extremely similar the published structure of murine QTRT2 (6FV5) [52]. Like the mouse protein, human QTRT2 overall resembles bacterial TGT or the catalytically active QTRT1, but the would-be active site region appears degenerate, as key residues and secondary structure elements are changed or missing.

Helix αA and β-sheet βD are absent in QTRT2 and the corresponding stretch encompassing residues 108 to 121 is without a secondary structure (Fig. 3). The course of this unfolded stretch partly diverges from that in the mouse QTRT2 structure (residues 101 to 107) and appears highly flexible as indicated by high atomic displacement parameters (ADPs). The reason for this is an unfavourable interaction with the equally flexible unpaired adenine 25 of a symmetry mate which is stacking with Y107 but directly interferes with the course of the preceding main chain as it is seen in the mouse structure (S 4). The subsequent βEβF sheet (residues 113–124), two-stranded due to the missing βD, is angled much closer to the centre of the subunit in QTRT2 (Fig. 3). Although it too exhibits locally increased ADPs, the position of the motif is identical to that of the mouse structure.

The structure of hTGT also confirms the presence of an additional small helix spanning residues 148–151 that we named α4a (Fig. 3). The area is rich in positively charged amino acid residues and makes crystal contact with the phosphate backbone of a symmetry related RNA (S 5) which forces it into a more indented conformation compared to the murine structure.

Finally, QTRT2 has an insertion of about 30 amino acid residues, however, as in the mouse structure, electron density for this insertion spanning residues 291 to 326 is completely missing, and we thus did not include it in model building.

Changes relating to heterodimerization are more subtle in QTRT2 compared to QTRT1 because the previously published mouse structure is that of a similarly configured homodimer [52]. Part of the β1α1-loop (residues 37 to 42) is shifted towards the interface to engage with QTRT1 residues 337–339. This also entails a minor change of the preceding α1 helix [42–53]. Similarly, the interface region 86–92 adopts a slightly altered conformation and the helix-turn-helix motif formed by helices αE and α8 of this subunit (residues 361–400) also shows a minor twist.

The dimer interface of QTRT1 and QTRT2

The structure of hTGT is the first crystallographic account of the dimer interface formed between eukaryotic QTRT1 and QTRT2. Dimerization mainly occurs via the two zinc-binding domains of the subunits and follows the overall architecture

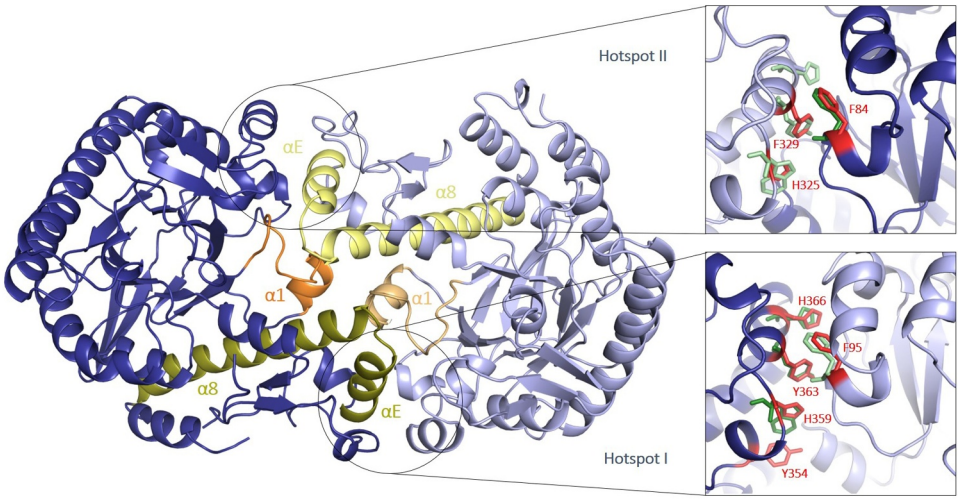

Figure 4. Dimer interface of QTRT1 and QTRT2.
The dimer interface of QTRT1 (light blue) and QTRT2 (dark blue) is primarily formed by two helix-turn-helix motifs (pale and dark yellow) interacting with two loop-helix motifs (light and dark orange) of the opposing subunit. The peripheries of the interface contain two aromatic hotspots. Hot spot residues are shown in red, corresponding residues from *Zymomonas mobilis* are shown in green for comparison.

of the bacterial homodimer: The interface is formed by two extensive helix-turn-helix motifs that consist of helices αE and α8 of both subunits interacting with the two loop-helix motifs comprised of the α1 helices and preceding β1α1 loops (Fig. 4).

The interface of hTGT also includes equivalents for the two characteristic aromatic hot spots of the bacterial homodimer [33,34]. Being a heterodimer, these two hot spots are not identical in eukaryotic TGT and will henceforth be referred to as hot spot (HS) I and II (Fig. 4).

HSI is comprised of QTRT1 F95 and QTRT2 residues H366, Y363 and H359. It thus has direct equivalents for the *Z. mobilis* residues F92, H333 and Y330. H359 occupies the position of the five-ring of *Z. mobilis* W326. The loss in hydrophobic area due to this change is compensated by the extension of the hot spot by an additional tyrosine (Y354).

HSII appears degenerate: Only QTRT1 F84 is conserved, F329 and H325 take the place of *Z. mobilis* Y330 and W326. There is no additional aromatic residue to compensate for the loss of the bulky tryptophan and *Z. mobilis* H333 is replaced by an alanine.

The two aromatic hot spots are located at the outer edges of the dimer interface, with most residues of the feature being provided by the two αE helices. The interior of the interface is characterized by a network of hydrogen bonds and polar interactions. Some of these interactions are formed by the hot spot residues themselves: In HSI, H366 and Y363 bond to the main chain carbonyls of Q51 and A52, consistent with their bacterial homologs. Because the equivalent residues (A332 and F329) have non-polar side chains, these interactions are lost in HSII.

In bacterial TGT, a key feature of the interface is the salt bridge between a glutamate sitting at the very apex of the helix-turn-helix motif and a lysine of the facing β1α1 loop (E339 and K52 in *Z. mobilis*). In human TGT, this interaction is conserved in the interface half containing HSI and formed between QTRT2 E372 and QTRT1 K55, although the terminal amide of QTRT1 Q51 is located at almost equal distance and might provide an additional hydrogen bond with E372. In the interface half of HSII, the apex region of the helix-turn-helix motif has a more extended conformation. As a result, an aspartate (D337) instead of a glutamate is sufficient to bond with K38 located in the N-terminal region of the QTRT2 β1α1 loop. This lysine is not the equivalent of *Z. mobilis* residue K52, instead it replaces the Q51 found in the first half of the interface. In addition, the interaction with the QTRT2 β1α1 loop in this second half of the interface is strengthened by QTRT1 N338 binding to several of its backbone functionalities as well as QTRT1 T339 bonding with QTRT2 H44.

Other interactions contributing to the polar interactions of the interface are QTRT2 Y354 (the additional tyrosine of HSI) bonding to the main-chain amide of QTRT1 E60, QTRT2 N358 binding QTRT1 N97 in the first half and QTRT1 H325 (part of HSII) bonding to QTRT2 H47 in the second half of the interface.

In the centre of the dimer interface, the two α1 helices of the subunits interact directly as QTRT1 E60 forms hydrogen bonds with the QTRT2 sidechains of H48 and N52.

Active site and binding of the RNA stem loop

The binding of the stem loop RNA substrate by human TGT appears to follow the model of the previously published bacterial complex [35]. The RNA is folded into a stem loop that is comprised of a stem of six helically stacked base pairs, a 5′ overhang of one base and a loop of seven unpaired nucleotides. The helical stem rests on the zinc-binding domain of the QTRT1 subunit, while the loop points into the C-terminal face of its $(\beta/\alpha)_8$ barrel core where the active site is located. As such, the RNA is bound almost exclusively by the QTRT1 subunit.

As reported for the bacterial RNA-complex, the loop region of the RNA adopts an unusual conformation which is quite different from that of the anticodon loop of a free tRNA: While the first unpaired base, C32, is roughly in plane with

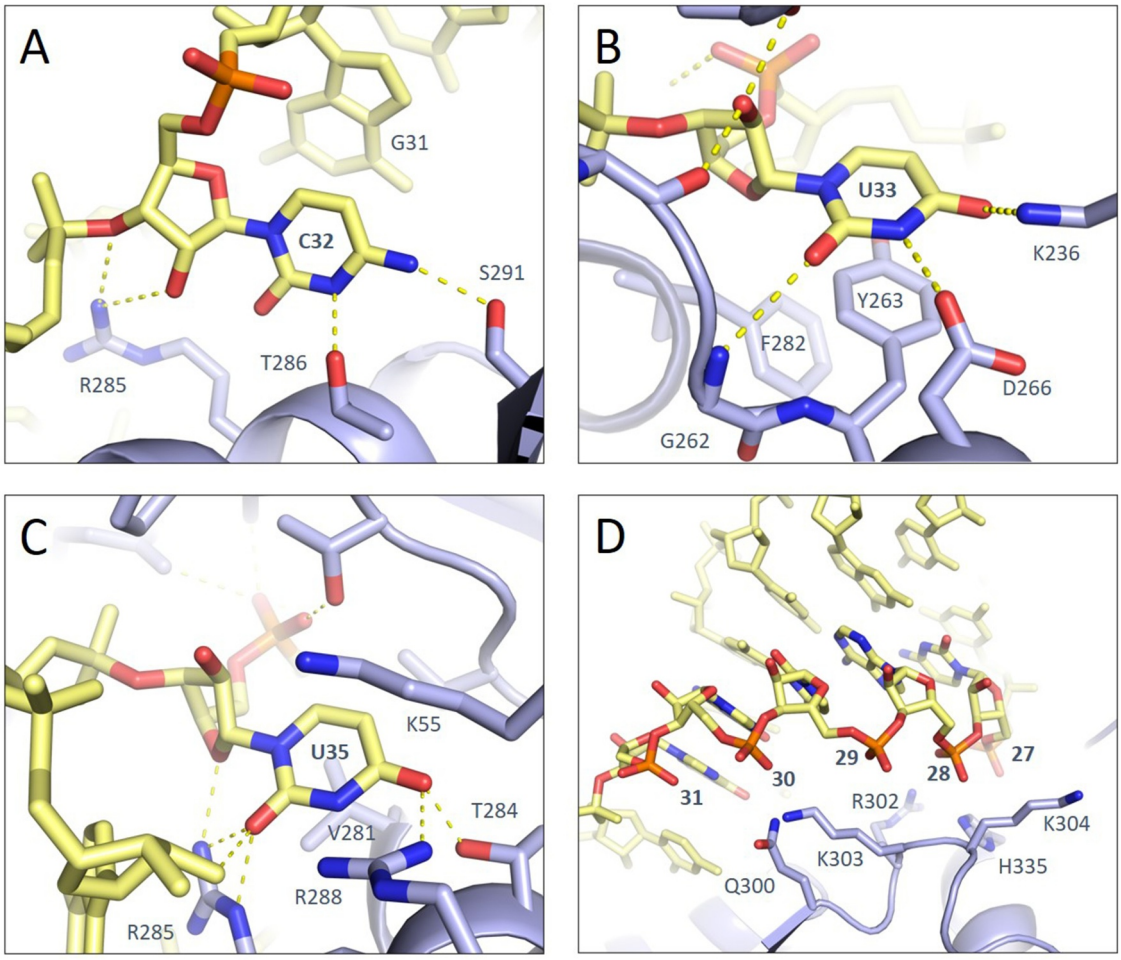

Figure 5. Sequence-specific and sequence-independent binding of RNA substrate.

RNA nucleotides are depicted in yellow stick representation, QTRT1 is depicted as cartoon and sticks in light blue. **A**: C32 forms weakly sequence-specific polar contacts with T286 and S291. **B**: U33 is stacked by Y263 and F282 and recognized specifically by K236, D266 and G262. **C**: C35 is stabilized between K55 and V281 and forms sequence-specific contacts with T284, R288 and R285. **D**: The helical stem of the RNA is bound sequence-independently via its negatively charged phosphate backbone. Nucleotides 27–31 (numbered) interact with positively charged QTRT1 residues Q300, K303, R302, H335 and K304.

the helical stacking of the stem, U33 is flipped out [35]. Nucleotides 35 to 38 are in a zig-zag conformation in which A36 and A38 are likewise flipped to the outside of the loop.

Knowing that bacterial TGTs recognize their RNA substrate by only the bases of the $Y_{32}U_{33}G_{34}U_{35}$ motif, it is of particular interest to see which bases of the loop are recognized in a sequence-specific manner by the human TGT. The first loop nucleotide, C32, is positioned only roughly in plane with the preceding helically stacked bases. It is stabilized in this position by forming a hydrogen bond with T286 and a polar interaction with S291 via its N3 and N4 nitrogens (Fig. 5A). This differs from the bacterial structure, where C32 is in plane with the helix stack and S291 is replaced by a glutamine.

U33 is stabilized in its flipped conformation via pi-stacking interaction with Y263, which is in turn stacked to F282. It accepts hydrogen bonds from K236 and the main-chain amide of G262 via its O2 and O4 carbonyl functions and forms an additional hydrogen bond with D266 via its N3 nitrogen (Fig. 5B). With the exception of K236, which does not exist in the bacterial protein, this way of binding is conserved, although the base is stabilized by hydrophobic packing with a lysine, not a tyrosine, in *Z. mobilis*.

The remnant ribose of G34 is covalently bound to D279 via its C1 atom, thus representing the covalent RNA-protein intermediate that is the result of the first half of the TGT reaction mechanism (Fig. 1B). D297 is held in place by its second terminal oxygen accepting a hydrogen bond from Y257. The C1 of ribose 34 is located at a distance of 4.2 Å from the C9 atom of the 9dzG base bound in the G/Q binding pocket, illustrating that a conformational change would be necessary for the formation of the new covalent bond and completion of the base exchange. The 9dzG base is stacked between M259 and F109, which is rotated slightly out of plane by the RNA-induced conformational change of αA. Specific recognition of the deazapurine occurs through several hydrogen bonds with its Watson–Crick Edge: The second catalytic aspartate D105 accepts a hydrogen bond from the N2, D159 accepts two more hydrogen bonds from the N1 and N2 and the O6 forms two hydrogen bonds with Q202 and the main-chain amine of G229.

U35 is stacked between K55 and V281. It forms specific contacts by its O4 accepting two hydrogen bonds from T284 and R288 and O2 accepting hydrogen bonds from R285, which also forms a second bond with the ribose O4′ of the same nucleotide (Fig. 5C). All of these interactions are conserved and have direct equivalents in the *Z. mobilis* structure.

While the flipped base A36 does not form any close contacts, A37 is stacked by R285 and R288 forms a hydrogen bond with O2′. A38 is the only base that is bound by two residues of the QTRT2 subunit: It is stabilized via hydrophobic interaction with L373 and polar interaction with N371. In the *Z. mobilis* structure, the stabilization of the base is achieved by an isoleucine at the same position. The polar interaction is formed with a main-chain carbonyl, but from both structures it seems unlikely that this single interaction is sufficient for sequence-specific recognition, especially in hTGT where the sidechain carbonyl is not at all held in position by any neighbouring residues.

Finally, QTRT1 F289 forms a stacking interaction with C39 thus holding it in position. As C39 and G31 form the first base pair of the stem, this interaction also serves to stabilize the helical stack. Unlike the loop, the helical stem is bound in a manner that is completely independent from sequence, mostly via its negatively charged phosphate backbone.

Due to the orientation of the stem loop, only the strand that includes nucleotides 26–30 makes contact with the protein, while the opposite strand (nucleotides 39–44) is positioned 'in mid-air'. The phosphate 30 forms two hydrogen bonds with K303 and Q300. The remaining phosphates of nucleotides 29–26 do not form dedicated hydrogen bonds. However, several positively charged or polar residues are located in the near vicinity (R302, K304 and H335), the closest at a distance of less than 5 Å (Fig. 5D).

Potential sites for tRNA binding

Inspection of the surface electrostatics of the heterodimer reveals that the RNA binding face exhibits two well-defined positively charged patches (Fig. 6). The first one extends from the active site to the zinc-binding domain of the QTRT1 subunit and represents the primary-binding site of the stem loop RNA. A second positively charged patch is located on the QTRT2 subunit, which is mostly formed by helices α4a and α4b. We prepared a model of the human $tRNA^{Asp}$ based on the published structure of its yeast equivalent (PDB-ID: 2TRA) and superimposed it to the helical stem of the RNA in the complex structure (S 6). In the resulting model, the acceptor stem of the aligned tRNA comes in close vicinity to the positively charged patch on the surface of QTRT2, suggesting that this patch binds the acceptor stem of a substrate tRNA via its negatively charged phosphate backbone.

According to the superimposed model, the two-stranded βEβF-sheet of the QTRT2 subunit also contributes to binding of the tRNA: Due to its complementary shape it is able to protrude into the groove that is formed by the tRNA's D-arm, where it is well positioned to form hydrogen bonds and Van der Waals interactions (Fig. 8A).

Analysis of UV-crosslinks of a TGT·tRNA complex

Aiming to gain experimental evidence for the involvement of the QTRT2 subunit in binding of a complete tRNA, we performed UV-induced crosslinking of a TGT·tRNA complex and analysed the crosslinked peptides using mass spectrometry. We identified 14 crosslinked peptides representing 12 unique crosslinks. However, many of the rarer crosslinks (<5 crosslink spectrum matches (CSMs)/replicate) are in locations that are biologically not plausible, such as the rear face of the dimer with respect to its active site. For that reason, we considered only those crosslinks with more than 5 CSMs in each replicate. We also excluded the two crosslinks at the QTRT1 and QTRT2 N-termini because we consider them to be artefacts caused by increased terminal flexibility. The remaining crosslinks involve QTRT1 residues G232, F289, Y131, K303 or 304 and QTRT2 residue W116 (Table 2). While the crosslinked QTRT1 residues are located around the crystallographically identified binding site of the stem loop RNA, QTRT2 W116 confirms the involvement of the βEβF-sheet of the non-catalytic subunit (Fig. 7). It was

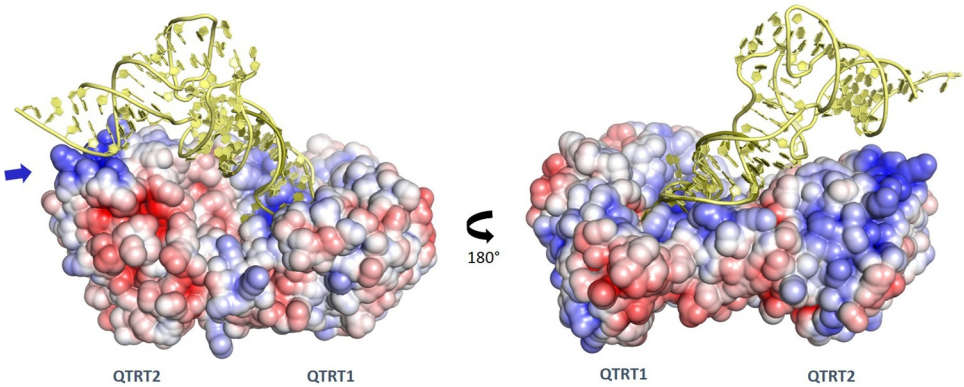

Figure 6. Surface electrostatics of the hTGT heterodimer and superimposed model of $tRNA^{Asp}$.

Two different views on the TGT heterodimer surface electrostatics (blue = positive charge, red = negative charge) are depicted. Two positively charged areas are visible: The first corresponds to the primary-binding site of the crystallized stem loop RNA (dark yellow), the second is located on the surface of the QTRT2 subunit (indicated by a blue arrow). A model of human $tRNA^{Asp}$ (light yellow) superimposed to the stem loop RNA comes in close contact to the positively charged area of QTRT2 via its acceptor stem.

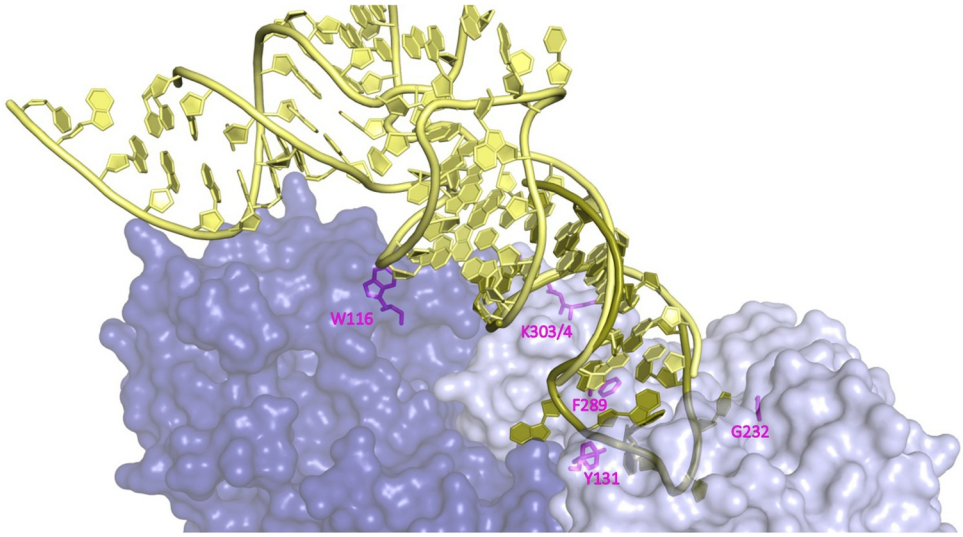

Figure 7. UV-Crosslinking of a TGT·tRNA complex.

Surface representation of QTRT1 (light blue) and QTRT2 (dark blue) with amino acid residues involved in crosslinks with $tRNA^{Asp}$ shown in magenta. The crystallized stem loop RNA is shown in dark yellow, a superimposed $tRNA^{Asp}$ model is shown in pale yellow.

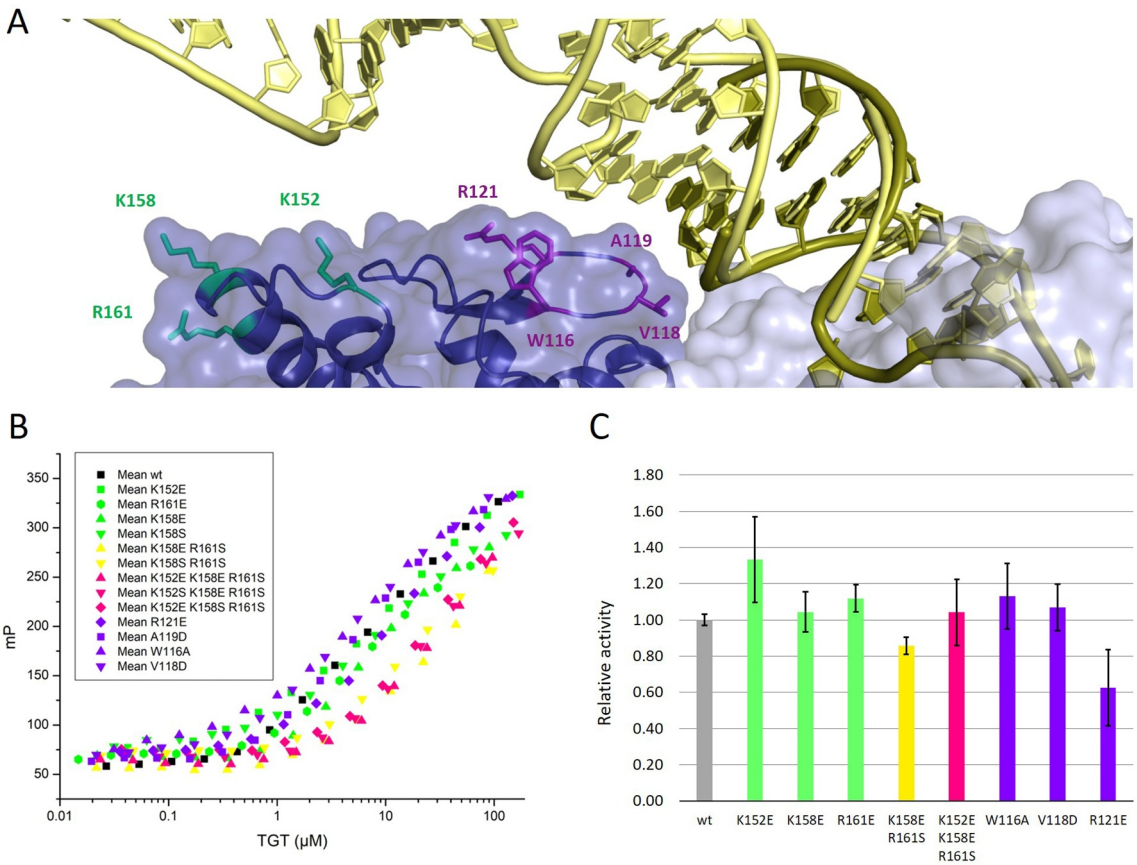

Figure 8. Mutagenesis of potential tRNA binding regions.

A: Surface representation of QTRT1 (light blue) and QTRT2 (dark blue) with stem-loop RNA (dark yellow) and a superimposed $tRNA^{Asp}$ model (pale yellow). Amino acid residues that underwent mutagenesis are shown as coloured stick representations (purple: βEβF-sheet, green: positively charged patch). **B**: Fluorescence polarization-based affinity assay with TGT mutants and labelled $tRNA^{Asp}$. Individual points represent the average of three triplicates, error bars were omitted for clarity. K_D values and their errors derived from each curve are listed in Table 3. **C**: Relative Q-incorporation activity of TGT mutants from three replicates with standard deviations shown as error bars.

Table 2. UV-crosslinking results

Peptide sequence[1]	CSMs in each replicate			>5	Position	Crosslinked base
	1	2	3			
MkLSLTK	11	19	16	Yes	QTRT2 K2	C
SVSVwSVAGR	11	18	13	Yes	QTRT2 W116	U
DVPGFAIGGLSgGESK	12	9	17	Yes	QTRT1 G232	U (C)[2]
gPMAGAATQASLESAPR	14	15	8	Yes	QTRT1 G-2	C
SPyDGNETLLSPEK	12	12	11	Yes	QTRT1 Y131	U
fGSALVPTGNLQLR	6	11	6	Yes	QTRT1 F289	C (U)[2]
FRSPyDGNETLLSPEK	4	7	6	No	QTRT1 Y131	U
kkVFEK	6	5	5	No	QTRT1 K303/4	C
kYQEDFNPLVR	5	6	5	No	QTRT2 K339	C
kVFEK	5	4	5	No	QTRT1 K304	C
lkNLGK	5	4	4	No	QTRT2 K18	C
LLSSVTAELPEDkPR	2	4	4	No	QTRT2 K247	C
LAQLkELIHR	1	4	5	No	QTRT2 K407	C
SDkLAQLK	2	3	4	No	QTRT2 K402	C

[1]Lower case letter represents crosslinked amino acid residue.
[2]Bases in parentheses represent a less abundant sub-population.

crosslinked exclusively to a uracil, corroborating the nearby placement of U11 in the superimposed tRNA model.

Mutagenesis of putative QTRT2 binding regions

To further investigate the involvement of the two suspected tRNA binding regions of the QTRT2 subunit, the βEβF-sheet and the positively charged patch involving helices α4a and α4b, we created a series of QTRT2 mutants. For the positively charged patch, we chose K152, K158 and R161 because they are solvent-exposed and do not interact with neighbouring residues in the hTGT structure and created single, double and triple mutants. The charge of each residue was either neutralized (mutation to serine) or inversed (mutation to glutamate), however, the combination of K158E and R161E resulted in presumably misfolded protein that could not be purified.

We tested the affinity with fluorescently labelled $tRNA^{Asp}$ and performed activity tests with each of the remaining mutants (Fig. 8). The affinity of the K158E and R161E single mutants was identical to that of the wildtype, for which we determined a K_D of 7.91 ± 0.86 μM (Table 3). The K152E and K158S mutants exhibited marginally reduced affinity with a less than 2-fold increased experimental K_D (12.51 ± 1.88 μM, 13.28 ± 3.54 μM). The binding curves of the K158S R161S and K158E R161S double mutants and K152E K158E R161S, K152S K158E R161S and K152E K158S R161S triple mutants were all noticeably shifted (Fig. 8B). Since these curves do not reach saturation, they could not be fitted, but upon visual inspection it is clear that the K_D of these mutants is well above 20 μM.

For the βEβF-sheet, we created the following single-point mutations: R121E, A119D, V118D and W116A. Mutants V118D and W116A were indistinguishable from the wildtype in affinity tests, the experimental K_D of the A119D mutant was marginally reduced (5.48 ± 0.42 μM). In contrast, the R121E mutation caused a 4-fold increased K_D (16.00 ± 1.09 μM).

We also determined the relative activity of some of the mutants (Fig. 8C). Despite the observed reduction of affinity of the double and triple mutants, the relative activity of all mutants of the positively charged patch deviated by less than 30% from that of the wildtype: The K158E R161S double mutant had activity reduced to 80% of that of the wildtype and the activity of the K152E single mutant was 1.3-fold increased, while all other mutants of the positively charged patch fell somewhere in between. The βEβF mutants W116A and V118D too had wildtype-like activity. With the relative activity reduced to 60% of the wildtype activity, the R121E mutation had the most drastic effect.

Discussion

Despite half a century of research on tRNA guanine transglycosylase (TGT), our understanding of eukaryotic TGT especially is still fragmentary. In this publication, we presented the first crystal structure of a eukaryotic TGT in its heterodimeric and RNA-bound form. With its aid, we were able to gain a thorough grasp of the functional elements that make up the interface of its two subunits. We were also able to analyse how a stem loop RNA is bound by eukaryotic TGT, make a conjecture on the binding of a full tRNA and evaluate whether and how it differs from bacterial TGT.

Comparing the subunits of the heterodimeric structure to the previously published apo-structures of the individual subunits, we saw several changes in conformation. The catalytic subunit QTRT1 was previously crystallized as an unusual homodimer in which both chains are aligned along their $(\beta/\alpha)_8$ barrels, an arrangement considered a crystallographic artefact by the authors [51]. QTRT2 was also crystallized as a homodimer, but it was configured similarly to the hTGT heterodimer. Unsurprisingly, the differences we observe in heterodimeric hTGT therefore mostly involve the regions of the dimer interface. However, most of these changes, such as the formation of QTRT1 helices α2a and α2b, are in line with structures of the bacterial TGT dimer. Like in bacterial TGT, the dimer association in eukaryotic TGT seems to be largely based on the interaction of its α1 helix and preceding β1α1 loop with a helix-turn-helix motif formed by helices αE and α8. Since the eukaryotic dimer interface exhibits a pseudo 2-fold symmetry, both of these elements occur twice. Looking at the two halves of the interface, it becomes clear

that they are unevenly conserved: The first half (involving the helix-turn-helix motif of QTRT2 and the loop-helix motif of QTRT1) is very similar to its bacterial homolog, including a salt bridge at the apex of the helix-turn-helix motif and the configuration of the aromatic hot spot which is thought to be the major contributor to dimer stability in bacterial TGT. In the second half, the interaction is stabilized by alternative bonds and the extent of the aromatic hot spot is significantly reduced. Interestingly, this reduction mostly effects the QTRT1 subunit, which contributes only three aromatic residues to the two hotspots, whereas QTRT2 contributes five. This might be the explanation why QTRT2 has previously been observed to form homodimers in solution, while QTRT1 has not [52].

The altered conformation of QTRT1 helix αA near the active site is the only major change that seems to be caused by the binding of the RNA substrate. It is shared only by the structures of the RNA-bound bacterial TGT [35]. The conformational change of αA causes a rotation of F109, which stacks the (deaza)purine in the active site and, in its rotated conformation, allows it to act like a lid to its binding pocket. This might be a mechanism of induced fit serving to shield the active site from water access and facilitating the nucleophilic attacks on ribose 34. While it is unclear whether the αA shift is induced by initial binding of the tRNA or whether it is the result of the conformational changes that occur during the formation of the covalent RNA-TGT intermediate, the former appears more likely: An equivalent αA conformation is also observed in the post-catalytic state of bacterial TGT bound to $preQ_{1\ 34}$-RNA, which is likely similar to the initial G_{34}-tRNA substrate complex [35]. In addition, conformational changes of the RNA occurring between the covalent intermediate and the formation of the post-catalytic state are limited to nucleotide 34 while the adenine at position 36, which is likely responsible for the shift of αA, occupies identical positions [35].

Recently, a sequential bi–bi mechanism in which queuine is bound before formation of an RNA-complex has been suggested for eukaryotic TGT instead of a ping-pong mechanism [58]. However, from the structure of hTGT it is clear that one base only, guanine 34 or queuine, can simultaneously reside at the active site. Even if, as the authors of the cited work suggest, queuine initially binds to a secondary binding site outside of the catalytic centre, a second queuine molecule would still need to bind to the active site after the freed guanine is released, which is why we continue to argue for a conserved ping-pong mechanism.

The RNA loop entering the active site groove in the hTGT complex structure has the same unusual conformation as described for the bacterial structure [35]. Nucleotides 33 and 35 are recognized by specific interactions that are largely the same as in the bacterial complex. C32 forms contacts with two sidechain hydroxyls, which likely could also bind a uracil in this position. So while we could show that eukaryotic TGT does not necessarily require an intact tRNA for its substrate, the hTGT structure confirms the previously shown importance of the $Y_{32}U_{33}G_{34}U_{35}$ sequence for recognition [56,57].

All nucleotides of the helical stem are bound via their phosphate backbone only, confirming that its sequence is unimportant for recognition. The helix is angled slightly differently to the bacterial structure. This might be caused by crystal contacts in either structure (in 1Q2R the helix stacks with its symmetry mate to form an extended helix, in the hTGT complex it binds to a positively charged region of QTRT2) or be related to the different angle of the βEβF motif of the QTRT2 subunit. This motif is part of the second large insertion in the $(\beta/\alpha)_8$ barrel fold and has already been identified as a potential contributor to tRNA binding in 2007 [59]. Back then, it was not yet known that eukaryotic TGT is a heterodimer of homologs, yet, the model based on the bacterial homodimer still holds up: The insertion comprised of residues 96–139 is heavily modified in QTRT2 compared to both QTRT1 and bacterial TGT, but while helix αA and subsequent βD strand are replaced by an unstructured stretch of amino acid residues, the two-stranded βEβF-sheet is conserved. By superimposing a model of human $tRNA^{Asp}$ to the stem loop RNA, we discovered that the motif is shaped perfectly for protruding into the groove formed by the tRNA's D-arm. UV-induced crosslinking of a TGT·tRNA complex confirmed the involvement of the βEβF motif. We created several mutants and showed that its R121E mutant has both decreased affinity with labelled $tRNA^{Asp}$ and reduced relative activity. Other mutants based on the motif were identical to the wildtype in these respects, however, this might either be due to the high flexibility in this area, allowing for the mutated residues to bend away from the RNA or because the previously hydrophobic interactions are replaced by polar contacts with its backbone.

The αA helix that is missing in QTRT2 is part of the active site in QTRT1 and bacterial TGT. Being a homodimer, it is also present in the noncatalytic subunit of the bacterial dimer, as the evolutionary pressure to keep the active site conserved likely much outweighs any potential benefits that might arise from optimizing the αA-βF insertion for tRNA binding. Through evolution of a noncatalytic homolog and the eukaryotic heterodimer, the insertion's function at the active site is decoupled from its role in tRNA binding, thus elevating this evolutionary pressure. Through the replacement of αA and βD with an unstructured loop, the now two-stranded βEβF-sheet is angled much less steeply than it is in bacteria, a conformation that is possibly more favourable for reaching into the tRNA's D-arm groove.

Table 3. Binding affinites of TGT mutants

TGT construct	Experimental K_D (μM)
wildtype	7.91 ± 0.86
QTRT2 K152E	12.51 ± 1.88
QTRT2 K158S	13.28 ± 3.54
QTRT2 K158E	7.83 ± 0.70
QTRT2 R161E	7.81 ± 1.68
QTRT2 K158S R161S	NA (>20)
QTRT2 K158E R161S	NA (>20)
QTRT2 K152E K158E R161S	NA (>20)
QTRT2 K152S K158E R161S	NA (>20)
QTRT2 K152E K158S R161S	NA (>20)
QTRT2 W116A	7.68 ± 0.73
QTRT2 V118D	7.68 ± 0.76
QTRT2 A119D	5.48 ± 0.42
QTRT2 R121E	16.00 ± 1.09

Through inspection of the surface electrostatics, we identified a striking concentration of positively charged residues in the α4a and α4b helices of the QTRT2 subunit. Its interaction with the stem loop of a symmetry mate RNA demonstrates the area's capability of binding the phosphate backbone of an RNA (S 5). In the superimposed model of a TGT·tRNA complex, the positively charged patch is in the vicinity of the tRNA's acceptor stem, but with a distance of approximately 10 Å, it is too far away to form polar contacts with its phosphate backbone. Our crosslinking experiments did not yield any evidence for the involvement of this area for tRNA binding. However, UV-induced crosslinking almost exclusively occurs with pyrimidine bases, so if the patch does bind the 3′ strand of the acceptor stem it would be unlikely to form crosslinks as human $tRNA^{Asp}$ exclusively contains purine bases in this area of the strand. The importance of this positively charged patch was corroborated by the observation that charge-inversed double and triple mutants of some of its positively charged residues had significantly reduced affinity with labelled $tRNA^{Asp}$. However, we also observed that the dual mutation of residues K158 and R161 to a glutamate resulted in presumably misfolded protein, likely because the two residues are located too closely together. Although we avoided mutating both residues to glutamate, all our double and triple mutants contain a combination of the two residues exchanged either for a serine or a glutamate. For this reason, it is possible that a local conformational change, while not rendering the protein insoluble, is the underlying reason for the observed loss in affinity.

The conformation of a tRNA is not static as is demonstrated by the inversed anticodon loop in RNA-bound TGT or the molten D-Arm in the structure of tRNA bound to another member of the TGT family, the archaeal protein inserting achaeosine into position 15 of the D-arm [60]. It is thus possible that a tRNA binding to the TGT heterodimer does adopt a bent conformation that allows its acceptor stem to make contact with the positively charged patch on the QTRT2 surface. However, while we are convinced of the involvement of the βEβF motif in tRNA binding, the experimental evidence is not sufficient to confidently say the same of the positively charged patch.

Finally, QTRT2 has a unique third insertion which appears disordered in both of its crystal structures. This putative loop of roughly 30 amino acid residues (292–326) has previously been proposed to play a role in orienting a substrate RNA and become ordered upon tRNA binding [52]. While we do not know if this is the case upon binding of a full tRNA, we consider it unlikely due to its remote location far away from both the stem loop RNA in the hTGT complex structure and the position of the superimposed tRNA. Instead, we speculate whether it could serve to anchor the TGT enzyme in the compartmentalized eukaryotic cell. Mitochondrial $tRNAs^{Asp,Asn,His,Tyr}$ are Q-modified in a QTRT1 and QTRT2-dependent manner and QTRT2 in particular has been associated with mitochondrial membranes [49,61], so the function of this QTRT2-specific insertion possibly could be to interact with a cellular structure or membrane-bound protein.

Materials and methods

Expression and purification of heterodimeric *H. sapiens* TGT

Human TGT was co-expressed and purified as a heterodimer (QTRT1 and QTRT2) essentially as described previously [51]. In brief, the proteins were co-expressed with a cleavable 6xHis-tag fused N-terminally to QTRT1 in *Escherichia coli* BL21 (DE3) cells using autoinduction medium (ZYM-5052 medium, 2 mM $MgSO_4$ replaced by 1 mM $MgCl_2$, supplemented with 100 mM $ZnCl_2$) [62]. Cells were initially grown for 3 h at 37°C followed by 50–60 h at 16°C before harvesting. Flash frozen cells were stored at −20°C. For purification, cells were thawed and disrupted using an ice-cold microfluidizer (M-110S Microfluidizer (Microfluidics, Westwood, MA, USA)) in 50 mM HEPES pH 7.5, 100 mM NaCl, 10 mM imidazole. The crude lysate was cleared by ultracentrifugation (1 h, 48,380 g, 4°C) and filtering through a 0.45 µM syringe filter (Filtropur (Sarstedt, Nümbrecht, Germany)). The cleared supernatant was loaded onto a Talon column (HiTrap TALON crude (GE Healthcare) or Clontech HisTALON Superflow (Takara Bio, Kusatsu, Japan)), washed with 1 M LiCl and target protein was eluted with 125 mM imidazole. All chromatographic steps were performed at 4°C. Pooled target protein was incubated with PreScission Protease (1:100 w/w) under mild agitation for 16–18 h at 4°C. Protein was concentrated using an Amicon ultrafiltration device (30 kDa MWCO, Merck) and further purified by Superdex S200 (GE Healthcare) size-exclusion chromatography (20 mM HEPES pH 7.5, 100 mM NaCl). TGT was concentrated to 7–10 mg/mL and, if not used directly, flash frozen in liquid nitrogen and stored at −80°C.

Crystallization, data collection and structure determination

Freshly purified TGT was mixed with 2-fold molar excess of synthetic stem loop RNA (sequence: AGCACGGCUGUAAACCGUGC, (Axolabs, Kulmbach, Germany)) and 5-fold excess 9-deazaguanine (AmBeed, Arlington Hts, IL, USA), diluted to a final protein concentration of 2 mg/mL and incubated on ice for 30 min. For crystallization, the complex solution was mixed 1:1 or 2:1 with screening conditions as sitting drops in a 3 Lens 96-well crystallization plate (SWISSCI, High Wycombe, UK) using a mosquito pipetting robot (SPT Labtech, Melbourn, UK). The crystallization plate was tightly sealed and incubated at either 4°C or 20°C. Crystals were harvested from 0.1 M MMT (DL malic acid, MES, Tris in 1:2:2 molar ratio) pH 6, 25% (w/v) PEG 1500 and 0.1 M Bis-Tris pH 5.5, 25% (w/v) PEG 3350 and 0.1 M sodium cacodylate pH 6.5, 25% (w/v) PEG 4000 after 3 months, where necessary cryoprotected with PEG 1500 (30% (w/v) final concentration, MMT grown crystals only) and stored in liquid nitrogen until further use.

X-ray diffraction data were collected at beamline MX 14.1 operated by the Helmholtz–Zentrum Berlin (HZB) at the BESSY II electron-storage ring, Berlin-Adlershof, Germany equipped with a PILATUS3 S 6 M detector. Diffraction images were indexed, integrated and scaled using the XDS-

package [63]. The structure the heterodimer was solved by molecular replacement with models 6H45 and 6FV5 (PDB-IDs) using PHASER [64]. Model adjustment, including placement of the RNA stem loop (PDB-ID: 1Q2R) and 9-deazaguanine, and building of QTRT2 residues divergent from the mouse protein was done in Coot [65]. Refmac05 was used for structure refinement in iterative cycles with manual model adjustment [66]. Atomic displacement parameters of the final model were refined using TLS parameterization in PHENIX [67].

Structural data representation and analysis

Structural figures were prepared using PyMol.

Surface electrostatics of the sidechain-completed hTGT heterodimer were calculated using the Adaptive Poisson-Boltzman method (APBS) as implemented within PyMOL [68].

Model of *H. sapiens* $tRNA^{Asp}$ and structure superposition

A model of human $tRNA^{Asp}$ was prepared based on the coordinates of *Saccharomyces cerevisiae* $tRNA^{Asp}$ (PDB-ID: 2TRA) by mutating the base sequence in Coot to fit the human tRNA. The tRNA model was superimposed to the TGT·RNA complex by aligning bases 25–31 and 39–42 in PyMOL.

In vitro transcription and purification of $tRNA^{Asp}$

Human $tRNA^{Asp}$ was transcribed *in vitro* from annealed DNA oligonucleotides (Merck) using T7 RNA polymerase (4 mM rNTPs, 25 mM $MgCl_2$, 1× HT buffer (30 mM HEPES pH 8.0, 10 mM DTT, 6 mM $MgCl_2$, 2 mM Spermidine, 0.01% Triton X-100)). The transcript was loaded onto a ResourceQ column (GE Healthcare) in 20 mM Hepes pH 7.5, 50 mM KCl and eluted in a shallow KCl gradient (245 to 732.5 mM in 150 mL). Fractions containing tRNA were pooled, precipitated with ethanol and the dried pellet dissolved in water.

Preparation of TGT·tRNA complex

TGT protein was mixed with 1.5-fold molar excess of $tRNA^{Asp}$ and incubated on ice for 30 min. The TGT·tRNA complex was purified by size-exclusion chromatography using a Sephadex 200 Increase 10/300 GL column (GE Healthcare) in 20 mM Hepes pH 7.5, 100 mM NaCl and concentrated to 1 mg/mL protein using an Amicon ultrafiltration device (30 kDa MWCO, Merck).

UV-crosslinking experiments were done in triplicates from three independently assembled and purified complex samples.

Protein-RNA crosslinking

For each replicate, 40 to 60 µg of purified TGT·tRNA complex were crosslinked by UV irradiation at 254 nm for 10 min on ice using an in-house built crosslinking apparatus as described in [69]. After ethanol-precipitation, the crosslinked complex was processed as described in [69] with minor modifications. Briefly, the protein-RNA pellet was dissolved in 4 M urea, 50 mM Tris/HCl, pH 7.5, following dilution to 1 M urea with 50 mM Tris/HCl, pH 7.5. Ten µg RNase A (EN0531, Thermo Fisher Scientific), 1kU RNase T1 (EN0531, Thermo Fisher Scientific) and 250 U PierceTM universal nuclease (88,700, Thermo Fisher Scientific) were added and $MgCl_2$ concentration was adjusted to 1 mM. RNA digestion was performed for 4 h at 37°C followed by protein digestion with trypsin (sequencing grade, Promega) at a 1:20 enzyme to protein mass ratio. Sample clean-up was performed using C18 columns (74–4601, Harvard Apparatus) and crosslinked peptides were enriched with in-house packed TiO2 columns (Titansphere 5 µm; GL Sciences, Japan) as described in [69]. Peptides were dried and subjected to MS measurement.

LC-MS/MS analysis and data analysis

Peptide pellets from TiO_2 enrichment were dissolved in 2% (v/v) acetonitrile, 0.05% (v/v) TFA. LC-MS/MS analyses were performed on a Q Exactive HF-X (Thermo Fisher Scientific) instrument coupled to a nanoflow liquid chromatography system (1100 series, Agilent Technologies). Sample separation was performed at a flow rate of 300 nl/min using a buffer system consisting of 0.1% (v/v) formic acid (buffer A) and 80% (v/v) acetonitrile, 0.08% (v/v) formic acid (buffer B) and linear gradient from 10% to 45% buffer B in 44 min. Peptides were separated over 58 min. Eluting heteroconjugates were analysed in positive mode using a data-dependent top 20 acquisition method. MS1 and MS2 resolution were set to 120,000 and 30,000 FWHM, respectively. AGC targets were set to 106 and 5×105, normalized collision energy (NCE) to 28%, dynamic exclusion to 21 s, and maximum injection time to 60 and 120 ms (MS1 and MS2). MS data were analysed and manually validated using the OpenMS pipeline RNPxl and OpenMS TOPPASViewer 1.

Mutagenesis

Site-directed mutagenesis was adapted from the supplier's protocol for the QuikChange Site-Directed Mutagenesis kit (Agilent) for using 35–45-mer DNA primers with a back-to-back overlap of 6–8 bases (Merck). Mutagenesis PCR (18 cycles, 54°C annealing temperature) was carried out with Phusion polymerase (Thermo Fisher Scientific).

Queuine incorporation activity tests

Queuine incorporation activity tests were based on the previously described boronate affinity electrophoresis, in which Q-containing RNA migrates more slowly due to interaction with its additional cis-diol [70]. The incorporation reaction was carried out in 10 µL volume: TGT (0.5 µM final concentration) was added to 4 µM of $tRNA^{Asp}$ in the presence of 1 mM queuine [9] in 100 mM HEPES pH 7.5, 20 mM MgCl2, 5 mM DTT. The reaction was incubated for 3 minutes at 37°C (after which approximately 50% substrate conversion is observed for the wildtype enzyme) and stopped by addition of an equal volume of RNA loading dye (New England

Biolabs). RNA samples were separated by affinity electrophoresis (120 V, 30 mA, 80 min, 4°C) in TAE buffer using gels prepared by supplementing the gel mixture (10% (w/v) acrylamide, 42% (w/v) urea) with 5 mg/mL 3-(acrylamido)phenylboronic acid (Merck) before polymerization. Gels were stained with GelRed (Biotium, Fremont, CA, USA), imaged and bands quantified using GelAnalyzer 19.1 (www.gelanalyzer.com). For each lane, the ratio of Q34 tRNA to total tRNA was determined (relative activity) and normalized by the wild-type value. The assay was performed in triplicates stemming from three independent incorporation reactions and affinity gels, with the exception of the R161E mutant for which only two replicates could be obtained.

tRNA labelling and fluorescence polarization affinity measurements

In vitro transcribed $tRNA^{Asp}$ was fluorescein-labelled as described previously [9]. For fluorescence polarization experiments, a two-fold dilution series of TGT (50 µL individual sample volumes) was mixed with 20 nM labelled tRNA in a black 96 well plate (Corning, Corning, NY, USA). Fluorescence polarization was measured after 5 minutes of shaking in a VICTOR Nivo plate reader (PerkinElmer). Triplicates were measured from three independent dilution series. Data evaluation and sigmoidal curve fitting were done with OriginPro 8.5.

Acknowledgments

We are grateful to the staff of beamline MS 14.1 at BESSYII/Helmholtz–Zentrum Berlin for allocation of beamtime and financial support. We would like to thank Piotr Neumann for the ample support regarding data collection and processing and continuous crystallographic advice. We are also thankful to Ulf Diederichsen and Matthias Krull for the synthesis of the queuine base. Further, we would like to thank Monika Raabe for help with the crosslink experiments and Klaus Reuter for fruitful discussion.

Funding

This work was supported with funding by the DFG (SPP1784, SFB860, Germany's Excellence Strategy—EXC 2067/1-390729940). We acknowledge support by the Open Access Publication Funds of the Göttingen University.

Data availability

Coordinates and diffraction data of the hTGT-RNA structure have been deposited within the Protein Data Bank (PDB ID 7NQ4).

Disclosure statement

No potential conflict of interest was reported by the author(s).

Author contributions

Experimental design (K.S., R.F.), protein expression and purification (K.S.), crystallography, data collection and structure determination (K.S.), crystal structure analysis (K.S.), tRNA purification and complex assembly (K.S.), crosslinking, mass spectrometry and crosslinking data analysis (L.W., under supervision by H.U.), mutagenesis and biochemical assays (K.S.), manuscript writing (K.S.), manuscript review and editing (K.S., R.F.).

ORCID

Ralf Ficner http://orcid.org/0000-0002-1739-6086

References

[1] Harada F, Nishimura S. Possible anticodon sequences of tRNAHis, tRNAAsn, and tRNAAsp from Escherichia coli. Universal presence of nucleoside Q in the first position of the anticodons of these transfer ribonucleic acids. Biochemistry. 1972;11:301–308.
[2] Meier F, Suter B, Grosjean H, et al. Queuosine modification of the wobble base in tRNAHis influences 'in vivo' decoding properties. Embo J. 1985;4:823–827.
[3] Zaborske JM, Bauer DuMont VL, Wallace EWJ, et al. A nutrient-driven tRNA modification alters translational fidelity and genome-wide protein coding across an animal genus. PLoS Biol. 2014;12:e1002015.
[4] Tuorto F, Legrand C, Cirzi C, et al. Queuosine-modified tRNAs confer nutritional control of protein translation. Embo J. 2018;37:e99777.
[5] Müller M, Legrand C, Tuorto F, et al. Queuine links translational control in eukaryotes to a micronutrient from bacteria. Nucleic Acids Res. 2019;47:3711–3727.
[6] Durand JMB, Dagberg B, Uhlin BE, et al. Transfer RNA modification, temperature and DNA superhelicity have a common target in the regulatory network of the virulence of Shigella flexneri: the expression of the virF gene. Mol Microbiol. 2000;35:924–935.
[7] Hurt JK, Olgen S, Garcia GA. Site-specific modification of Shigella flexneri virF mRNA by tRNA-guanine transglycosylase in vitro. Nucleic Acids Res. 2007;35:4905–4913.
[8] Müller M, Hartmann M, Schuster I, et al. Dynamic modulation of Dnmt2-dependent tRNA methylation by the micronutrient queuine. Nucleic Acids Res. 2015;43:10952–10962.
[9] Johannsson S, Neumann P, Wulf A, et al. Structural insights into the stimulation of S. pombe Dnmt2 catalytic efficiency by the tRNA nucleoside queuosine. Sci Rep. 2018;8:8880.
[10] Wang X, Matuszek Z, Huang Y, et al. Queuosine modification protects cognate tRNAs against ribonuclease cleavage. RNA. 2018;24:1305–1313.
[11] Kasai H, Ohashi Z, Harada F, et al. Structure of the modified nucleoside Q isolated from Escherichia coli transfer ribonucleic acid. 7-(4,5-cis-dihydroxy-1-cyclopenten-3-ylaminomethyl)-7-deazaguanosine. Biochemistry. 1975;14:4198–4208.
[12] Yokoyama S, Miyazawa T, Iitaka Y, et al. Three-dimensional structure of hyper-modified nucleoside Q located in the wobbling position of tRNA. Nature. 1979;282:107–109.
[13] Phillips G, Yacoubi BE, Lyons B, et al. Biosynthesis of 7-deazaguanosine-modified tRNA nucleosides: a new role for GTP cyclohydrolase I. J Bacteriol. 2008;190:7876–7884.
[14] McCarty RM, Somogyi Á, Bandarian V. Escherichia coli QueD Is a 6-carboxy-5,6,7,8-tetrahydropterin Synthase. Biochemistry. 2009;48:2301–2303.
[15] McCarty RM, Somogyi Á, Lin G, et al. The deazapurine biosynthetic pathway revealed: in vitro enzymatic synthesis of PreQ0 from guanosine 5′-triphosphate in four steps. Biochemistry. 2009;48:3847–3852.
[16] Dowling DP, Bruender NA, Young AP, et al. Radical SAM enzyme QueE defines a new minimal core fold and metal-dependent mechanism. Nat Chem Biol. 2014;10:106–112.
[17] Van Lanen SG, Reader JS, Swairjo MA, et al. From cyclohydrolase to oxidoreductase: discovery of nitrile reductase activity in a common fold. Proc Natl Acad Sci. 2005;102:4264–4269.
[18] Lee BWK, Van Lanen SG, Iwata-Reuyl D. Mechanistic studies of bacillus subtilis QueF, the nitrile oxidoreductase involved in queuosine biosynthesis. Biochemistry. 2007;46:12844–12854.
[19] Chikwana VM, Stec B, Lee BWK, et al. Structural basis of biological nitrile reduction. J Biol Chem. 2012;287:30560–30570.

[20] Okada N, Noguchi S, Kasai H, et al. Novel mechanism of post-transcriptional modification of tRNA. Insertion of bases of Q precursors into tRNA by a specific tRNA transglycosylase reaction. J Biol Chem. 1979;254:3067–3073.
[21] Okada N, Nishimura S. Isolation and characterization of a guanine insertion enzyme, a specific tRNA transglycosylase, from Escherichia coli. J Biol Chem. 1979;254:3061–3066.
[22] Slany RK, Bösl M, Kersten H. Transfer and isomerization of the ribose moiety of AdoMet during the biosynthesis of queuosine tRNAs, a new unique reaction catalyzed by the QueA protein from Escherichia coli. Biochimie. 1994;76:389–393.
[23] Mathews I, Schwarzenbacher R, McMullan D, *et al*. Crystal structure of S-adenosylmethionine: tRNAribosyltransferase-isomerase (QueA) from thermotoga maritima at 2.0 Å resolution reveals a new fold. Proteins Struct Funct Bioinforma. 2005;59:869–874.
[24] Grimm C, Ficner R, Sgraja T, et al. Crystal structure of bacillus subtilis S-adenosylmethionine: tRNAribosyltransferase-isomerase. Biochem Biophys Res Commun. 2006;351:695–701.
[25] Van Lanen SG, Iwata-Reuyl D. Kinetic mechanism of the tRNA-modifying enzyme S-adenosylmethionine: tRNARibosyltransferase-isomerase (QueA). Biochemistry. 2003;42:5312–5320.
[26] Frey B, McCloskey J, Kersten W, et al. New function of vitamin B12: cobamide-dependent reduction of epoxyqueuosine to queuosine in tRNAs of Escherichia coli and salmonella typhimurium. J Bacteriol. 1988;170:2078–2082.
[27] Miles ZD, McCarty RM, Molnar G, et al. Discovery of epoxyqueuosine (oQ) reductase reveals parallels between halorespiration and tRNA modification. Proc Natl Acad Sci. 2011;108:7368–7372.
[28] Payne KAP, Fisher K, Sjuts H, et al. Epoxyqueuosine reductase structure suggests a mechanism for cobalamin-dependent tRNA modification. J Biol Chem. 2015;290:27572–27581.
[29] Dowling DP, Miles ZD, Köhrer C, et al. Molecular basis of cobalamin-dependent RNA modification. Nucleic Acids Res. 2016;44:9965–9976.
[30] Romier C, Reuter K, Suck D, et al. Crystal structure of tRNA-guanine transglycosylase: RNA modification by base exchange. Embo J. 1996;15:2850–2857.
[31] Chong S, Curnow AW, Huston TJ, et al. tRNA-guanine transglycosylase from Escherichia coli is a zinc metalloprotein. Site-directed mutagenesis studies to identify the zinc ligands. Biochemistry. 1995;34:3694–3701.
[32] Immekus F, Barandun LJ, Betz M, et al. Launching spiking ligands into a protein–protein interface: a promising strategy to destabilize and break interface formation in a tRNA modifying enzyme. ACS Chem Biol. 2013;8:1163–1178.
[33] Jakobi S, Nguyen TXP, Debaene F, et al. Hot-spot analysis to dissect the functional protein–protein interface of a tRNA-modifying enzyme. Proteins Struct Funct Bioinforma. 2014;82:2713–2732.
[34] Jakobi S, Nguyen PTX, Debaene F, et al. What glues a homodimer together: systematic analysis of the stabilizing effect of an aromatic hot spot in the protein–protein interface of the tRNA-modifying enzyme Tgt. ACS Chem Biol. 2015;10:1897–1907.
[35] Xie W, Liu X, Huang RH. Chemical trapping and crystal structure of a catalytic tRNA guanine transglycosylase covalent intermediate. Nat Struct Mol Biol. 2003;10:781–788.
[36] Ritschel T, Atmanene C, Reuter K, et al. An integrative approach combining noncovalent mass spectrometry, enzyme kinetics and X-ray crystallography to decipher Tgt protein-protein and protein-RNA interaction. J Mol Biol. 2009;393:833–847.
[37] Goodenough-Lashua DM, Garcia GA. tRNA–guanine transglycosylase from E. coli: a ping-pong kinetic mechanism is consistent with nucleophilic catalysis. Bioorganic Chem. 2003;31:331–344.
[38] Reyniers JP, Pleasants JR, Wostmann BS, et al. Administration of exogenous queuine is essential for the biosynthesis of the queuosine-containing transfer RNAs in the mouse. J Biol Chem. 1981;256:11591–11594.
[39] Ott G, Kersten H, Nishimura S. Dictyostelium discoideum: a useful model system to evaluate the function of queuine and of the Q-family of tRNAs. FEBS Lett. 1982;146:311–314.
[40] Katze JR, Gunduz U, Smith DL, et al. Evidence that the nucleic acid base queuine is incorporated intact into tRNA by animal cells. Biochemistry. 1984;23:1171–1176.
[41] Kirtland GM, Morris TD, Moore PH, et al. Novel salvage of queuine from queuosine and absence of queuine synthesis in chlorella pyrenoidosa and chlamydomonas reinhardtii. J Bacteriol. 1988;170:5633–5641.
[42] Siard TJ, Jacobson KB, Farkas WR. Queuine metabolism and cadmium toxicity in drosophila melanogaster. BioFactors Oxf Engl. 1991;3:41–47.
[43] Gaur R, Björk GR, Tuck S, et al. Diet-dependent depletion of queuosine in tRNAs in caenorhabditis elegans does not lead to a developmental block. J Biosci. 2007;32:747–754.
[44] Shindo-Okada N, Okada N, Ohgi T, et al. Transfer ribonucleic acid guanine transglycosylase isolated from rat liver. Biochemistry. 1980;19:395–400.
[45] Katze BB, McCloskey JA. Queuine, a modified base incorporated posttranscriptionally into eukaryotic transfer RNA: wide distribution in nature. Science. 1982;216:55–56.
[46] Chen Y-C, Brooks AF, Goodenough-Lashua DM, et al. Evolution of eukaryal tRNA-guanine transglycosylase: insight gained from the heterocyclic substrate recognition by the wild-type and mutant human and Escherichia coli tRNA-guanine transglycosylases. Nucleic Acids Res. 2011;39:2834–2844.
[47] Kasai H, Nakanishi K, Macfarlane RD, et al. The structure of Q* nucleoside isolated from rabbit liver transfer ribonucleic acid. J Am Chem Soc. 1976;98:5044–5046.
[48] Okada N, Shindo-Okada N, Nishimura S. Isolation of mammalian tRNAAsp and tRNATyr by lectin-sepharose affinity column chromatography. Nucleic Acids Res. 1977;4:415–423.
[49] Boland C, Hayes P, Santa-Maria I, et al. Queuosine formation in eukaryotic tRNA occurs via a mitochondria-localized heteromeric transglycosylase. J Biol Chem. 2009;284:18218–18227.
[50] Chen YC, Kelly VP, Stachura SV, et al. Characterization of the human tRNA-guanine transglycosylase: confirmation of the heterodimeric subunit structure. RNA. 2010;16:958–968.
[51] Johannsson S, Neumann P, Ficner R. Crystal structure of the human tRNA guanine transglycosylase catalytic subunit QTRT1. Biomolecules. 2018;8:81.
[52] Behrens C, Biela I, Petiot-Bécard S, et al. Homodimer architecture of QTRT2, the noncatalytic subunit of the eukaryotic tRNA-guanine transglycosylase. Biochemistry. 2018;57:3953–3965.
[53] Müller SO, Slany RK. Structural analysis of the interaction of the tRNA modifying enzymes Tgt and QueA with a substrate tRNA. FEBS Lett. 1995;361:259–264.
[54] Curnow AW, Kung FL, Koch KA, et al. tRNA-guanine transglycosylase from Escherichia coli: gross tRNA structural requirements for recognition. Biochemistry. 1993;32:5239–5246.
[55] Nakanishi S, Ueda T, Hori H, et al. A UGU sequence in the anticodon loop is a minimum requirement for recognition by escherichia coli tRNA-guanine transglycosylase. J Biol Chem. 1994;269:32221–32225.
[56] Carbon P, Haumont E, Fournier M, et al. Site-directed in vitro replacement of nucleosides in the anticodon loop of tRNA: application to the study of structural requirements for queuine insertase activity. Embo J. 1983;2:1093–1097.
[57] Grosjean H, Edqvist J, Stråby KB, et al. Enzymatic formation of modified nucleosides in tRNA: dependence on tRNA architecture. J Mol Biol. 1996;255:67–85.
[58] Alqasem MA, Fergus C, Southern JM, et al. The eukaryotic tRNA-guanine transglycosylase enzyme inserts queuine into tRNA via a sequential bi–bi mechanism. Chem Commun. 2020;56:3915–3918.
[59] Stengl B, Meyer EA, Heine A, et al. Crystal structures of tRNA-guanine transglycosylase (TGT) in complex with novel and potent inhibitors unravel pronounced induced-fit adaptations and suggest dimer formation upon substrate binding. J Mol Biol. 2007;370:492–511.
[60] Ishitani R, Nureki O, Nameki N, et al. Alternative tertiary structure of tRNA for recognition by a posttranscriptional modification enzyme. Cell. 2003;113:383–394.

[61] Suzuki T, Yashiro Y, Kikuchi I, *et al*. Complete chemical structures of human mitochondrial tRNAs. Nat Commun. 2020;11:4269.
[62] Studier FW. Protein production by auto-induction in high-density shaking cultures. Protein Expr Purif. 2005;41:207–234.
[63] Kabsch W. XDS. Acta Crystallogr D Biol Crystallogr. 2010;66:125–132.
[64] McCoy AJ, Grosse-Kunstleve RW, Adams PD, et al. Phaser crystallographic software. J Appl Crystallogr. 2007;40:658–674.
[65] Emsley P, Lohkamp B, Scott WG, et al. Features and development of coot. Acta Crystallogr D Biol Crystallogr. 2010;66:486–501.
[66] Murshudov GN, Skubák P, Lebedev AA, et al. REFMAC5 for the refinement of macromolecular crystal structures. Acta Crystallogr D Biol Crystallogr. 2011;67:355–367.
[67] Adams PD, Afonine PV, Bunkóczi G, *et al*. PHENIX: a comprehensive Python-based system for macromolecular structure solution. Acta Crystallogr D Biol Crystallogr. 2010;66:213–221.
[68] Jurrus E, Engel D, Star K, *et al*. Improvements to the APBS biomolecular solvation software suite. Protein Sci Publ Protein Soc. 2018;27:112–128.
[69] Kramer K, Sachsenberg T, Beckmann BM, et al. Photo-cross-linking and high-resolution mass spectrometry for assignment of RNA-binding sites in RNA-binding proteins. Nat Methods. 2014;11:1064–1070.
[70] Igloi GL, Kössel H. Affinity electrophoresis for monitoring terminal phosphorylation and the presence of queuosine in RNA. Application of polyacrylamide containing a covalently bound boronic acid. Nucleic Acids Res. 1985;13:6881–6898.